

Photoionization of multishell fullerenes studied by ab initio and model approaches

[Eur. Phys. J. D 70 (2016) 221]

Alexey Verkhovtsev,^{1,2,*} Andrei V. Korol,^{1,3} and Andrey V. Solov'yov^{1,†}

¹*MBN Research Center, Altenhöferallee 3, 60438 Frankfurt am Main, Germany*

²*Instituto de Física Fundamental, CSIC, Serrano 113-bis, 28006 Madrid, Spain*

³*St. Petersburg State Maritime Technical University,
Leninskii ave. 101, 198262 St. Petersburg, Russia*

Photoionization of two buckyonions, $C_{60}@C_{240}$ and $C_{20}@C_{60}$, is investigated by means of time-dependent density-functional theory (TDDFT). The TDDFT-based photoabsorption spectrum of $C_{60}@C_{240}$, calculated in a broad photon energy range, resembles the sum of spectra of the two isolated fullerenes, thus illustrating the absence of strong plasmonic coupling between the fullerenes which was proposed earlier. The calculated spectrum of the smaller buckyonion, $C_{20}@C_{60}$, differs significantly from the sum of the cross sections of the individual fullerenes because of strong geometrical distortion of the system. The contribution of collective electron excitations arising in individual fullerenes is evaluated by means of plasmon resonance approximation (PRA). An extension of the PRA formalism is presented, which allows for the study of collective electron excitations in multishell fullerenes under photon impact. An advanced analysis of photoionization of buckyonions, performed using modern computational and analytical approaches, provides valuable information on the response of complex molecular systems to the external electromagnetic field.

I. INTRODUCTION

Formation and dynamics of electron excitations in fullerenes, their derivatives and other carbon-based nanoscale systems like polycyclic aromatic hydrocarbons (PAHs) have been widely studied, both experimentally and theoretically, during the past decades [1–6]. A particular attention has been paid to ionization of a C_{60} fullerene under the photon, electron, and ion impact [7–14]. Because of their high symmetry and stability, these molecules have been of significant fundamental interest aimed at better understanding the photon- and charged-particle-induced processes in complex many-particle systems. The understanding of the mechanisms of electron emission from nanoscale systems exposed to ionizing radiation is a key issue in a wide range of physical and chemical processes [15, 16].

Although the structure and dynamics of pristine fullerenes have been widely explored, much less attention has been paid to more complex systems, namely multishell fullerenes or buckyonions – concentric carbon nanostructures composed of several nested molecules [17, 18]. Unlike fullerenes and carbon nanotubes, the properties of carbon buckyonions are still not well understood. Accurate theoretical studies of the structure and dynamical properties of these systems are also rather limited because of the large number of constituent atoms and related high computational costs.

Several papers have been devoted to the study of the

static dipole polarizability of carbon buckyonions [19, 20]. Density-functional theory (DFT) calculations [20] revealed that the static dipole polarizability of the $C_{60}@C_{240}$ onion is very similar to that of the isolated C_{240} , so that the inner fullerene is almost completely screened by the outer shell. References [21, 22] were devoted to a theoretical study of photoionization and photoelectron angular distribution asymmetry parameters of an atom A confined in spherical multiwalled fullerenes, $A@C_{60}@C_{240}$ and $A@C_{60}@C_{240}@C_{540}$. In these works, the electronic structure of a confined atom was calculated explicitly, e.g., within the Hartree-Fock approximation, while the fullerene shells were modeled by a set of spherical zero- or finite-width attractive potentials.

Finally, only a few works have investigated photoabsorption spectra of buckyonions [23–25]. Similar to pristine fullerenes, nanotubes and PAHs, photoabsorption and electron energy loss spectra of buckyonions are characterized by prominent plasmon resonances formed due to collective excitations of delocalized σ and π electrons [26, 27]. In Ref. [23], Ruiz *et al.* presented a theoretical model for the calculation of the photoabsorption spectra of spherical N -shell carbon buckyonions in the low photon energy region (below 10 eV) dominated by the π -plasmon. The effect due to the π -plasmon was evaluated in this model based on the electronic structure of the system provided by the Hückel single-electron model. In Ref. [24], the photoionization of a bilayer $C_{60}@C_{240}$ onion was studied by means of the time-dependent local-density approximation, while the jellium model, that is, a uniform smearing of the valence electron density over a finite-width spherical shell, was used to represent the electronic structure of each fullerene. The calculated photoionization spectrum of $C_{60}@C_{240}$ showed a significant redistribution of the oscillator strength density and the emergence of two new resonances, as compared to the sum of the cross sections of the pristine systems. These

* verkhovtsev@iff.csic.es; On leave from A.F. Ioffe Physical-Technical Institute of Russian Academy of Sciences, Politekhnicheskaya 26, 194021 St. Petersburg, Russia

† On leave from A.F. Ioffe Physical-Technical Institute of Russian Academy of Sciences, Politekhnicheskaya 26, 194021 St. Petersburg, Russia

effects were explained in terms of a strong inter-fullerene coupling leading to hybridization of the electronic states of individual fullerenes and the formation of four cross-over plasmons [24]. In a recent work [25], the photoabsorption spectra of $C_{60}@C_{240}$ and $C_{60}@C_{180}$ onions were calculated by means of time-dependent DFT (TDDFT) in the visible-near UV region (up to 5 eV). The resulting spectrum of $C_{60}@C_{240}$ was characterized by a simple overlap of the spectra of isolated C_{60} and C_{240} because of a weak mutual perturbation of the two fullerenes upon encapsulation.

In this paper, we evaluate the photoabsorption spectra of two buckyonions, $C_{60}@C_{240}$ and $C_{20}@C_{60}$, by means of the two complementary theoretical approaches. The TDDFT method is used to calculate the spectra in a broad photon energy range up to 100 eV. The results of TDDFT-based calculations are compared with those based on the plasmon resonance approximation (PRA) [3, 4, 28] in order to map the well-resolved features of the spectra to particular collective electron excitations. The PRA formalism is extended allowing for the study of collective electron excitations in multishell fullerenes under photon impact. We demonstrate that the spectrum of the $C_{60}@C_{240}$ buckyonion corresponds to the sum of the spectra of the two isolated fullerenes, thus indicating the absence of strong inter-fullerene coupling. On the contrary, the photoabsorption spectrum of $C_{20}@C_{60}$ differs significantly from the corresponding sum of the isolated molecules due to strong geometrical distortion of the system. These results provide valuable information about a fundamental problem of the formation and interplay of collective electron excitations in complex nanoscale systems.

The atomic system of units, $m_e = |e| = \hbar = 1$, is used throughout the paper unless otherwise indicated.

II. THEORY AND COMPUTATIONAL DETAILS

A. Time-dependent density-functional theory

The TDDFT-based calculations of isolated fullerenes and buckyonions have been performed in the linear regime within the dipole approximation [29, 30]. Within this framework, the external potential $v_{\text{ext}}(\mathbf{r}, t)$ acting on a system is represented as a sum of a time-independent part, $v_{\text{ext}}^0(\mathbf{r})$, and a time-dependent perturbation $v'_{\text{ext}}(\mathbf{r}, t)$. The time evolution of the electron density, $\rho(\mathbf{r}, t)$, is then represented as a sum of the unperturbed ground-state density, $\rho_0(\mathbf{r})$, and the variation $\delta\rho(\mathbf{r}, t)$, which arises due to $v'_{\text{ext}}(\mathbf{r}, t)$.

Performing the Fourier transform of time-dependent quantities, one gets the response of the system to an external perturbation in the frequency representation. For the external perturbation $v'_{\text{ext}}(\mathbf{r}, \omega) = -\mathbf{E}(\omega) \cdot \mathbf{r}$ due to a uniform electric field, the Fourier transform of the in-

duced dipole moment reads as follows:

$$d_i(\omega) = \sum_j \alpha_{ij}(\omega) E_j(\omega), \quad (1)$$

where i, j denote the Cartesian components, $\alpha_{ij}(\omega)$ is the dynamical polarizability tensor which describes the linear response of the dipole to the external electric field:

$$\alpha_{ij}(\omega) = - \int r_i \chi(\mathbf{r}, \mathbf{r}', \omega) r'_j d\mathbf{r} d\mathbf{r}', \quad (2)$$

$\chi(\mathbf{r}, \mathbf{r}', \omega)$ is the generalized frequency-dependent susceptibility of the system, and r_i and r'_j are the components of the position operators \mathbf{r} and \mathbf{r}' . The photoabsorption cross section is related to the imaginary part of $\alpha_{ij}(\omega)$ through

$$\sigma(\omega) = \frac{4\pi\omega}{3c} \sum_j \text{Im} [\alpha_{jj}(\omega)], \quad (3)$$

where c is the speed of light, and the summation is performed over the diagonal elements of the polarizability tensor.

The performed calculations rely on the approach introduced in Refs. [29, 30], which is based on a superoperator formulation of TDDFT. It allows for the calculation of the dynamic polarizability by means of an efficient Lanczos method. In this approach, the polarizability of a many-electron system is expressed as [31]:

$$\alpha_{ij}(\omega) = \text{Tr} \left(\hat{X}_i \hat{\rho}'_j(\omega) \right), \quad (4)$$

where the hat symbols indicate quantum mechanical operators, \hat{X}_i is the i th component of the position operator \hat{X} , and $\hat{\rho}'_j(\omega) = \hat{\rho}_j(\omega) - \hat{\rho}_0$ is the response density matrix. It is expressed via $\hat{\rho}_j(\omega)$, that is the single-electron density matrix of the system perturbed by an external homogeneous electric field polarized along the j th axis, and $\hat{\rho}_0$, that is the density matrix describing the ground state. The response density matrix can be expressed as the solution of the linearized quantum Liouville equation [29, 30, 32]:

$$(\omega - \mathcal{L}) \cdot \hat{\rho}'_j(\omega) = [\hat{X}_j, \hat{\rho}_0], \quad (5)$$

where \mathcal{L} is the so-called Liouvillian operator and the square brackets indicate a commutator. The action of the Liouvillian \mathcal{L} onto $\hat{\rho}'(\omega)$ is defined as

$$\mathcal{L} \cdot \hat{\rho}'(\omega) = [\hat{H}_0, \hat{\rho}'(\omega)] + [\hat{V}'_{\text{Hxc}}[\hat{\rho}'], \hat{\rho}_0], \quad (6)$$

where \hat{H}_0 is the ground-state Kohn-Sham Hamiltonian calculated within the DFT approach and $\hat{V}'_{\text{Hxc}}[\hat{\rho}]$ denotes the linear variation of the electrostatic and exchange-correlation potentials. The coordinate representation of the latter operator is as follows:

$$v'_{\text{Hxc}}(\mathbf{r}, \omega) = \int \left(\frac{1}{|\mathbf{r} - \mathbf{r}'|} + \kappa_{\text{xc}}(\mathbf{r}, \mathbf{r}'; \omega) \right) \rho'(\mathbf{r}, \mathbf{r}'; \omega) d\mathbf{r}', \quad (7)$$

and κ_{xc} is the so-called exchange-correlation kernel. The polarizability tensor (4) is defined from the solution of Eq. (5) as the off-diagonal matrix element of the resolvent of the Liouvillian \mathcal{L} . In the approach introduced in Refs. [30–32], this quantity is calculated using the Lanczos recursion method (for details, see the above cited papers and references therein).

In this study, photoabsorption spectra of pristine and multishell fullerenes were obtained for the systems with optimized geometries. The optimization procedure was performed by means of Gaussian 09 package [33] utilizing the split-valence 6-31G(d) basis set and the local density approximation (LDA) [34]. The photoabsorption spectra of the optimized systems were obtained using the TDDFPT module [31] of the QuantumEspresso package [35]. The optimized structures were introduced into a supercell of $20 \times 20 \times 20 \text{ \AA}^3$. Then, the system of Kohn-Sham equations was solved self-consistently for all valence electrons ($2s^2 2p^2$ electron in each carbon atom) of each system to calculate the ground-state eigenvalues using a plane-wave approach [35]. In the calculations, we used an ultrasoft pseudopotential [36] which substitutes real atomic orbitals in the core region with smooth nodeless pseudo-orbitals. For the plane-wave calculations we used the kinetic energy cutoff of 30 Ry for the wave functions and 180 Ry for the electron densities.

B. Plasmon resonance approximation

The contribution of plasmon excitations to the photoabsorption spectra of isolated fullerenes has been evaluated using the plasmon resonance approximation (PRA) [3, 4, 28]. Within this approach, a single fullerene is represented as a spherically symmetric system with a homogeneous charge distribution within the shell of a finite width, $\Delta R = R_2 - R_1$, where $R_{1,2}$ are the inner and the outer radii of the molecule, respectively [37–41]. In other words, a fullerene is modeled as a system with the electron density being constant inside the spherical shell and equal to zero outside the shell. The chosen value of the shell's width, $\Delta R = 1.5 \text{ \AA}$, corresponds to the typical size of the carbon atom [38] and was successfully utilized in our earlier studies, see, e.g., Refs. [11, 40, 42]. A question of validity of the rectangular electron density profile and its comparison with more realistic densities in C_{60} was addressed in a number of earlier studies, see, e.g., Refs. [43, 44]. In these works, it was found that the shape of the electron density distributions does not affect the overall shape and the peak positions of the imaginary part of the dipole polarizability and hence the photoionization cross section.

Within the PRA, the dynamical polarizability $\alpha(\omega)$ has a resonance behavior in the region of frequencies where collective electron modes in a fullerene can be excited. Due to interaction with the uniform external field, $\mathbf{E}(\omega)$, the variation of the electron density, $\delta\rho(\mathbf{r}, \omega)$, occurs on the inner and outer surfaces of the fullerene shell.

This variation leads to the formation of the surface plasmon, which has two normal modes of vibration, the symmetric (s) and antisymmetric (a) ones [37–39, 45]. Hence, the cross section, $\sigma(\omega) \propto \text{Im } \alpha(\omega)$, is defined as

$$\sigma(\omega) = \frac{4\pi\omega^2}{c} \times \left[\frac{N_s \Gamma_s}{(\omega^2 - \omega_s^2)^2 + \omega^2 \Gamma_s^2} + \frac{N_a \Gamma_a}{(\omega^2 - \omega_a^2)^2 + \omega^2 \Gamma_a^2} \right], \quad (8)$$

where ω is the photon energy, ω_s and ω_a are the resonance frequencies of the two plasmon modes, Γ_s and Γ_a are the corresponding widths, and N_s and N_a are the number of delocalized electrons, involved in each collective excitation mode. The latter values obey the sum rule $N_s + N_a = N$, where N stands for a total number of delocalized electrons in the fullerene. In the present study, we account for the both π and $(\sigma + \pi)$ plasmons, which involve only π or both $\sigma + \pi$ delocalized electrons of the system, respectively. Thus, the photoionization cross section is defined as $\sigma(\omega) = \sigma^\pi(\omega) + \sigma^{\sigma+\pi}(\omega)$, where the contribution of each plasmon is governed by the two modes, as follows from Eq. (8). The frequencies of the collective excitations are defined as [37, 38]:

$$\begin{aligned} (\omega_{s/a}^{\sigma+\pi})^2 &= \omega_0^2 + \frac{N^{\sigma+\pi}}{2R_2^3(1-\xi^3)} \left(3 \mp \sqrt{1+8\xi^3} \right) \\ (\omega_{s/a}^\pi)^2 &= \frac{N^\pi}{2R_2^3(1-\xi^3)} \left(3 \mp \sqrt{1+8\xi^3} \right), \quad (9) \end{aligned}$$

where the signs '−' and '+' correspond to the symmetric and antisymmetric modes, respectively, and $\xi = R_1/R_2$ is the ratio of the inner to the outer radii. The quantities $N^{\sigma+\pi} = N_s^{\sigma+\pi} + N_a^{\sigma+\pi}$ and $N^\pi = N_s^\pi + N_a^\pi$ are the number of delocalized electrons involved in the formation of the $(\sigma + \pi)$ - and π -plasmons, respectively; their sum is equal to the total number of delocalized electrons in the fullerene, N . The parameter ω_0 comes from the Lorentz model of insulators and accounts for bound electrons in the case of the $(\sigma + \pi)$ plasmon [38]. This parameter defines a threshold above which the free-electron picture of the charge density becomes fully applicable. Below ω_0 , some of the valence electrons are treated as bound ones and, therefore, are not involved in the formation of the plasmon excitation. In this representation, frequency-dependent dielectric function is defined as $\epsilon(\omega) = 1 + \omega_p^2/(\omega_0^2 - \omega^2)$ with ω_p^2 being the volume plasmon frequency defined by the equilibrium distribution of electron density; it is expressed in terms of the total number of delocalized electrons and the volume of the fullerene shell, $\omega_p^2 = 3N/(R_2^3 - R_1^3)$. In this case, valence electrons are assumed to be bound to their local sites by an average, isotropic force proportional to ω_0^2 [37]. Therefore, only the π electrons are active for photon energies below the threshold ω_0 . Above this value, all $(\sigma + \pi)$ electrons become active and should be taken into consideration. In the present calculations, we have utilized the value of $\omega_0 = 13 \text{ eV}$ which was suggested in Ref. [37] to reproduce the strong absorption peak in the

spectrum of C_{60} around 20 eV [7]. In Ref. [38], a similar value of $\omega_0 = 14$ eV was proposed as an average energy of $\sigma - \sigma^*$ transitions between the bonding and antibonding bands of carbon nanosystems with sp^2 -hybridization. When considering the contribution of the π -plasmon, the parameter ω_0 is set to zero.

In this study, we have also extended the above described formalism to investigate collective electron excitations in multishell fullerenes under photon impact. The general methodology for analyzing plasmon excitations formed in buckyonions is presented in Appendix A. In this extension, the behavior of electron density on each fullerene is governed by the coupling parameter which is introduced according to geometry of the system. This parameter stands for the separation distance between the outer surface of the j th fullerene and the inner surface of the $(j + 1)$ th fullerene. In Appendix B, this methodology is applied to the case of $C_{60}@C_{240}$ and its current limitations are outlined.

III. RESULTS

A. Photoionization of $C_{60}@C_{240}$

Figure 1 demonstrates the photoabsorption spectrum of a $C_{60}@C_{240}$ buckyonion calculated within the TDDFT approach in the photon energy region up to 100 eV (thick black curve). The sum of the cross sections of isolated C_{60} and C_{240} fullerenes, $\sigma(\omega)_{C_{60}} + \sigma(\omega)_{C_{240}}$, is shown by the thin red curve, while the constituents of this sum are presented in the inset. In what follows, this sum is denoted as $\sigma(C_{60} + C_{240})$ for simplicity. The figure demonstrates that the cross section of the buckyonion is quite similar to that of the two isolated fullerenes. In the photon energy range between 10 and 20 eV, the spectrum of the buckyonion almost coincides with $\sigma(C_{60} + C_{240})$, while a slight difference between the two spectra appears above 20 eV. This difference is due to a 10-15% variation of oscillator strength and its redistribution from the high-energy region, at about 40 eV, to the region around 20 eV in the case of the buckyonion. The general similarity between the calculated TDDFT-based spectrum of $C_{60}@C_{240}$ and the sum $\sigma(C_{60} + C_{240})$ indicates the absence of strong plasmonic coupling between individual fullerenes which was proposed earlier based on the jellium model [24].

The difference between our results and those reported in Ref. [24] may be attributed to a different treatment of the ionic subsystem. In the cited work, the ionic core of each fullerene comprising the buckyonion was treated as a uniform distribution of the positive charge over a spherical shell of a finite width. On the contrary, in this work, we treat all carbon ions explicitly accounting for the icosahedral symmetry of both C_{60} and C_{240} , and that of the $C_{60}@C_{240}$ buckyonion, as well as for their structural optimization.

To investigate the obtained results in more detail, we

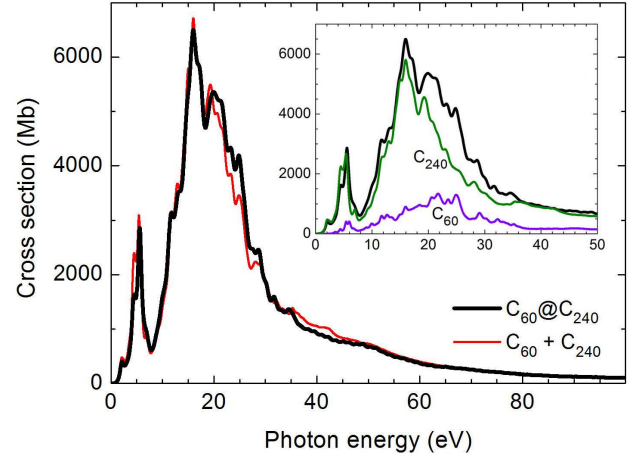


FIG. 1. The photoabsorption cross section of a $C_{60}@C_{240}$ buckyonion calculated within the TDDFT method (thick black curve). Spectra of the isolated C_{60} and C_{240} fullerenes are shown in the inset. The cross section $\sigma(C_{60} + C_{240})$ which is the sum of the latter two is shown by a thin red line.

have analyzed the radial distribution of valence electron density in the buckyonion and compared it to the distribution in pristine fullerenes, see Fig. 2. In the case of a fullerene C_n , the number N of delocalized electrons represents the four $2s^2 2p^2$ valence electrons from each carbon atom. Thus, the figure illustrates the contribution of 240, 960, and 1200 electrons in C_{60} , C_{240} , and $C_{60}@C_{240}$, respectively. To calculate the density distribution, we have adopted the procedure, utilized previously in Ref. [46]. Briefly, the electron density $\rho(\mathbf{r})$ created by the delocalized electrons of each system, was extracted from the Gaussian output .chk file with the help of the Multiwfn software, ver. 3.3.8 [47]. The density included only delocalized electrons, while the inner electron orbitals ($1s^2$ electrons from each atom) were excluded from consideration. Then, the electron density was averaged over the directions of the position vector \mathbf{r} :

$$\bar{\rho}(r) = \frac{1}{4\pi} \int \rho(\mathbf{r}) d\Omega. \quad (10)$$

Figure 2 demonstrates that the valence electron density in the buckyonion (solid black curve) almost coincides with that of the two pristine fullerenes (symbols). As follows from the performed DFT calculations, the electronic structure of the buckyonion remains almost unperturbed, compared to the isolated systems. The binding energies of the highest-occupied molecular orbital (HOMO) and the lowest valence MO are 5.3/24.3 eV in $C_{60}@C_{240}$, as compared with 5.7/24.3 eV in C_{60} and 5.3/24.0 eV in C_{240} . Thus, encapsulation of C_{60} into C_{240} does not affect the electronic properties of the latter one and its response to the external field. This is in agreement with the results of recent DFT-based calculations, which revealed that the dipole polarizability of $C_{60}@C_{240}$ is only about 1.8% higher than that of the isolated C_{240} [48]. The spatial separation of the electron density on each fullerene in

the buckyunion results in a minor alteration of the photoabsorption cross section of $C_{60}@C_{240}$ as compared to the sum $\sigma(C_{60} + C_{240})$.

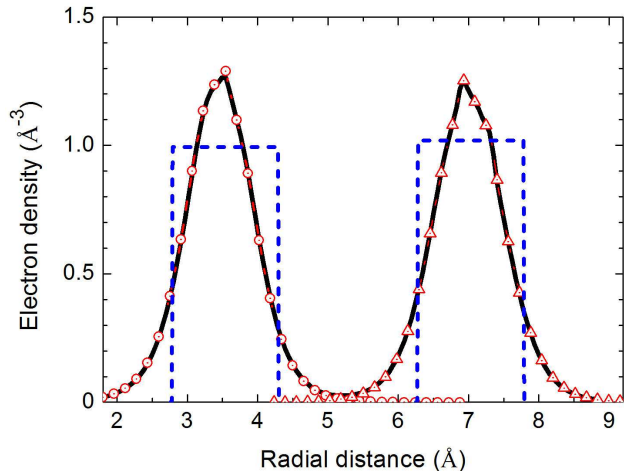


FIG. 2. Radial dependence of electron density $\bar{\rho}(r)$: density distribution of 1200 delocalized electrons in $C_{60}@C_{240}$ (solid black curve) and that of 240 and 960 electrons in pristine C_{60} and C_{240} , respectively (symbols). Dashed profile shows the model density distribution considered within the PRA (see the text for further details).

Similar to the case of pristine C_{240} , the TDDFT-based spectrum of the buckyunion is characterized by a prominent resonance peak centered at about 18 eV, which is actually split into two narrower peaks having maximum values at 16 and 20.5 eV (see the inset of Fig. 1). This feature can be explained by the electronic structure of the larger fullerene, namely by a dense distribution of single-electron energy levels having ionization potential of about 10-15 eV, as follows from the performed DFT calculations. In Ref. [42], the well-resolved features in the photoabsorption spectrum of C_{60} were assigned to discrete transitions between particular molecular orbitals (MOs) of the fullerene, reflecting its high symmetry, and to the ionization of particular molecular orbitals of the system. A similar explanation should hold for the description of the two-peak profile in the spectrum of C_{240} ; however, a detailed analysis of the electronic structure of this system goes beyond the scope of the present paper. Both C_{60} and C_{240} have icosahedral symmetry so that their MOs are classified according to the I_h irreducible representations. The MOs are singly (a_g, a_u), triply (t_{1g}, t_{1u}), (t_{2g}, t_{2u}), fourfold (g_g, g_u), and fivefold (h_g, h_u) degenerated with the subscripts “g” and “u” denoting, respectively, symmetric (“gerade”) and anti-symmetric (“ungerade”) MOs with respect to the center of inversion of the molecule.

Due to the quasispherical structure of the C_{60} and C_{240} molecules, their MOs can be expanded in terms of spherical harmonics in the angular momentum l [42, 50]. For instance, the innermost valence a_g , t_{1u} , and h_g MOs in the I_h symmetry represent, respectively, the s , p , and d

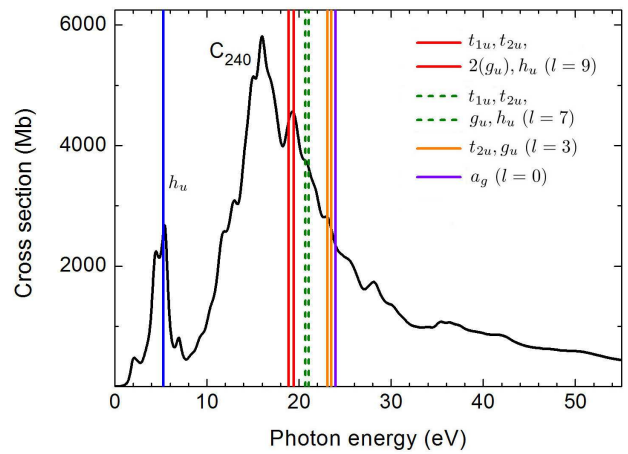


FIG. 3. The photoabsorption cross section of C_{240} calculated by means of TDDFT (black curve). Vertical lines denote ionization thresholds of the HOMO, h_u , as well as of a number of innermost valence MOs of the fullerene, as calculated at 6-31G(d)/LDA level of theory. The ionization thresholds for the HOMO (h_u) and the innermost valence (a_g) MOs are equal to 5.3 and 24.0 eV, respectively.

orbitals, which correspond to $l = 0, 1$, and 2. The orbitals which correspond to higher angular momenta are constructed as a combination of several MOs (see, e.g., Table 2 in Ref. [42]). In Fig. 3, we present ionization thresholds of several particular orbitals of C_{240} which are depicted by vertical lines. The electronic structure of C_{240} , although being much more dense, is quite similar to that of C_{60} . For the latter molecule, we demonstrated previously [42] that there are no discrete optical transitions with the energy above 20 eV, so that a series of peaks and bumps, arising between 20 and 25 eV, can be assigned to the ionization of the innermost valence MOs. As noted above, the DFT calculations for C_{240} , performed at 6-31G(d)/LDA level of theory, yield the ionization potentials of the HOMO, h_u , and the innermost valence MO, a_g , equal to 5.3 and 24.0 eV, respectively. Thus, the features of the spectrum of C_{240} in this photon energy range can be attributed to optically allowed discrete transitions (resulting in the change of the MO’s symmetry, $g \leftrightarrow u$) and to the ionization of particular MOs of the system.

B. Plasmons in C_{60} and C_{240}

Figure 4 shows the contribution of plasmon excitations to the cross section of isolated C_{60} and C_{240} , evaluated by means of the formalism presented in Section II B. The utilized parameters of the model are summarized in Table I. In the performed analysis, we assumed that the ratio $\gamma = \Gamma/\omega$ of the width of the $(\sigma+\pi)$ -plasmon resonance to its frequency is equal to $\gamma_s = 0.6$ for the symmetric mode, and to $\gamma_a = 1.0$ for the antisymmetric mode [11]. These values have been utilized earlier to describe experi-

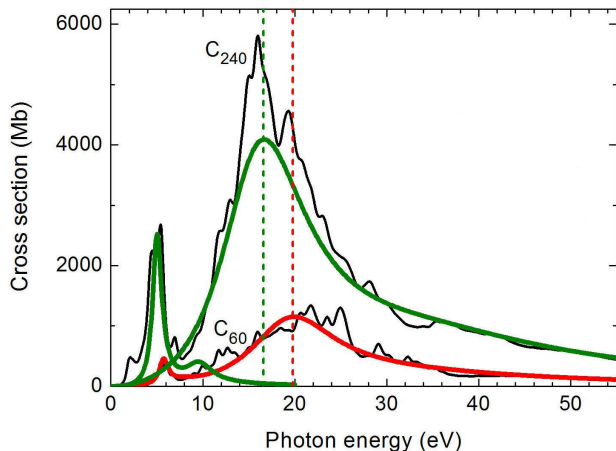


FIG. 4. Contribution of the plasmon excitations to the photoabsorption cross section of C_{60} (red curve) and C_{240} (green curves) fullerenes, calculated by means of the PRA. The curves, obtained within the classical approach, describe the dominating plasmon resonance, which is formed due to collective oscillations of σ and π delocalized electrons of the systems, and a narrow low-energy peak below 10 eV is attributed to the collective excitation of only π electrons. Dashed vertical lines indicate the plasmon resonance frequencies ω_s in the case of the two isolated fullerenes (see Table I).

mental data on photoionization [49] and electron inelastic scattering [11, 40] of gas-phase C_{60} . The value $\gamma_s = 0.6$ is also close to the numbers obtained from the earlier photoionization and electron energy loss experiments on neutral C_{60} [7, 10]. The value $\gamma_a = 1.0$ is consistent with the widths of the second plasmon resonance observed in the photoionization of C_{60}^{q+} ($q = 1 - 3$) ions [9]. Since there is no information available in the literature about the plasmon resonance widths in C_{240} , we have utilized the same ratios, $\gamma_s = 0.6$ and $\gamma_a = 1.0$, as in the case of C_{60} .

Figure 4 demonstrates that the PRA quantitatively describes the main features of the spectra reasonably well. The main resonant structure in the spectrum of each fullerene is formed due to the collective excitation of both σ and π electrons, while a prominent peak in the low-energy region of the spectrum (below 10 eV) is attributed to the excitation of some fraction of π electrons. Analysis of the plasmon contribution revealed that about 9 and 60 π -electrons (out of 60 and 240 in C_{60} and C_{240} , respectively) are involved in the low-energy collective excitation. The maximum of the $(\sigma + \pi)$ -plasmon resonance peak for the larger fullerene is about 3.2 eV lower than that in C_{60} because of a larger size of the molecule.

The oscillator strengths for C_{240} , calculated by means of TDDFT and within the PRA in the photon energy range up to 100 eV, are equal to 895 and 854, respectively. The level of accuracy of the present calculations is similar to the earlier calculations done for C_{60} [42], where the oscillator strengths in the region up to 100 eV were estimated as 224 and 195, respectively. In the cited

TABLE I. Properties of the C_{60} and C_{240} fullerenes: the total number of valence electrons, N , the mean radius, R , the inner/outer radii, $R_{1,2} = R \pm \Delta R/2$ for the thickness $\Delta R = 1.5$ Å, the ratio $\xi = R_1/R_2$, the surface plasmon energies ω_s and ω_a calculated from Eq. (9), and the corresponding widths Γ_s and Γ_a , calculated for the high-energy $(\sigma + \pi)$ -plasmon and for the low-energy π -plasmon. Widths for the π -plasmon are taken from Ref. [42].

Fullerene	C_{60}	C_{240}
N	240	960
R (Å)	3.54	7.07
R_1 (Å)	2.75	6.32
R_2 (Å)	4.25	7.82
ξ	0.65	0.81
$\omega_s^{(\sigma+\pi)}$ (eV)	19.8	16.6
$\omega_a^{(\sigma+\pi)}$ (eV)	34.6	35.7
$\Gamma_s^{(\sigma+\pi)}$ (eV)	11.9	10.0
$\Gamma_a^{(\sigma+\pi)}$ (eV)	34.6	35.7
ω_s^π (eV)	5.7	5.0
ω_a^π (eV)	8.0	9.6
Γ_s^π (eV)	1.2	[42]
Γ_a^π (eV)	3.5	[42]

paper, this difference was attributed to the contribution from single-particle excitations, which are neglected in the model. For the photon energies above 100 eV, the remaining oscillator strengths are due to ionization of individual carbon atoms, multiplied by 240 and 60, respectively. This contribution can be evaluated utilizing the asymptotic dependence of the dipole polarizability in the region of large photon frequencies, $\alpha(\omega) \propto -1/\omega^2$ [51].

C. Photoionization of $C_{20}@C_{60}$

As analyzed above, the electronic and geometrical properties of $C_{60}@C_{240}$ do not change much as compared to the corresponding constituents. However, it is not the case for $C_{20}@C_{60}$, the smallest and one of the simplest possible buckyonions, which we have also analyzed in this work. The stability as well as geometrical and electronic properties of this system were studied earlier by means of semi-empirical, Hartree-Fock and DFT calculations [52, 53]. The composite system was found to be a highly endothermic but stable structure possessing lower symmetry compared to its isolated constituents.

The TDDFT-based cross section for $C_{20}@C_{60}$ is presented in Figure 5 (thick black curve). Contrary to the case of $C_{60}@C_{240}$, the resulting spectrum of the smaller buckyonion differs significantly from the corresponding sum of the cross sections of isolated C_{60} and C_{20} (thin red curve). The reason for this difference is that the core of the outer fullerene becomes strongly distorted upon encapsulation of the smaller molecule. In the optimized

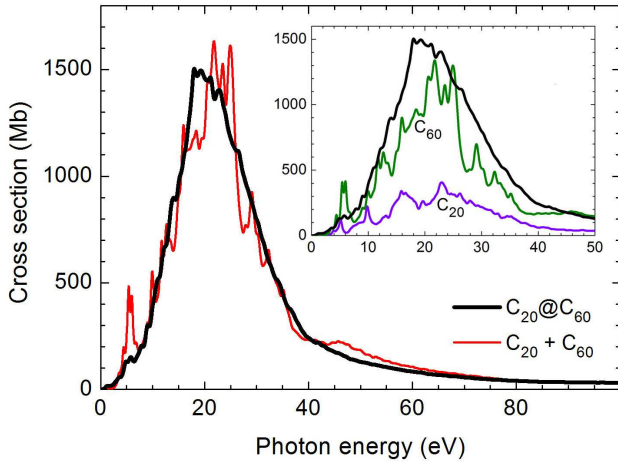


FIG. 5. The photoabsorption cross section of a $C_{20}@C_{60}$ buckyion calculated within the TDDFT method (thick black line). Spectra of isolated fullerenes C_{20} and C_{60} are shown in the inset. The cross section $\sigma(C_{20} + C_{60})$ which is a sum of the latter two is shown by a thin red line.

configuration for $C_{20}@C_{60}$, 20 atoms of C_{60} are located in the vicinity of their initial positions and form covalent bonds with the atoms of the smaller fullerene, while the other atoms of C_{60} are pushed away from their equilibrium position in the isolated molecule by about 0.4 Å. This happens because of a small inter-layer separation ($R_{C_{20}} = 2.04$ Å and $R_{C_{60}} = 3.54$ Å) that is comparable with the length of a C–C single bond in the systems with sp^2 -hybridization, $R_{C-C} = 1.47$ Å [55]. Because of the fact that in $C_{20}@C_{60}$ the atoms of C_{20} form covalent bonds with the atoms of the C_{60} cage, this structure has been suggested to be considered as a carbon cluster rather than a multishell fullerene [54].

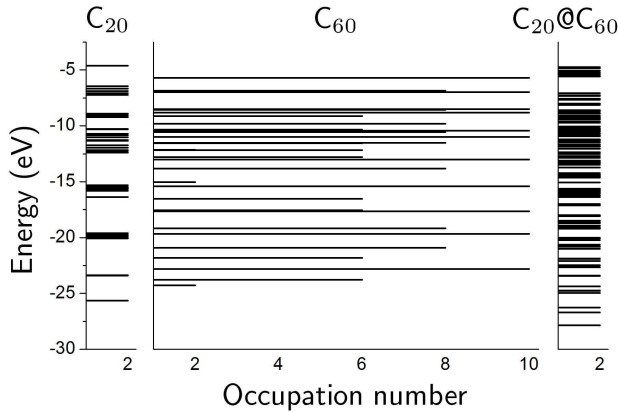


FIG. 6. The ground-state electronic structure of C_{20} , C_{60} and of $C_{20}@C_{60}$ buckyion, obtained within the quantum-mechanical framework accounting for the real symmetry of the systems.

Geometrical distortion of the buckyion leads to a significant rearrangement of its electronic structure, which

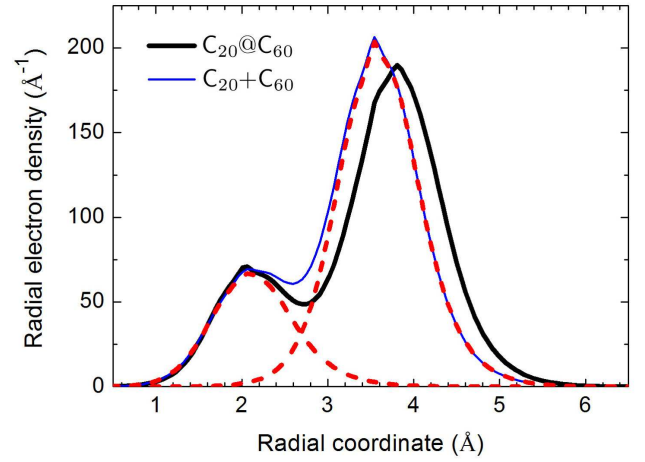


FIG. 7. Radial distribution of the radial electron density, $4\pi r^2 \bar{\rho}(r)$, associated with the valence electrons in the $C_{20}@C_{60}$ (solid black curve) and in the pristine C_{20} and C_{60} molecules (dashed red curves). The sum of the latter two is shown by a thin solid (blue) curve.

is illustrated in Fig. 6. To further support this statement, we analyzed the distribution of the valence electron density, see Fig. 7. Note that, in order to emphasize the effect, we have plotted not the average electron density $\bar{\rho}(r)$ but the radial density, $4\pi r^2 \bar{\rho}(r)$. The radial density distribution reflects an increase of the volume of $C_{20}@C_{60}$ compared to C_{60} . As a consequence, the valence electron density in the buckyion, associated with C_{60} , is shifted further from the geometrical center of the system. The alteration of the electron density results in the complete disappearance of the π -plasmon below 10 eV and smearing out of the fine structure atop the $(\sigma + \pi)$ -plasmon (see Fig. 5). Distortion of the buckyion geometry leads to a strong reduction of symmetry, so that the fine features, associated with discrete transitions between particular MOs of C_{60} , smear out into a smoother profile.

IV. CONCLUSION

This work has been devoted to the investigation of photoionization of multishell fullerenes. Time-dependent density-functional theory was utilized to calculate the photoabsorption spectra of $C_{60}@C_{240}$ and $C_{20}@C_{60}$ in a broad photon energy range up to 100 eV. Apart from a minor redistribution (of 10-15%) of the oscillator strength, the calculated spectrum of $C_{60}@C_{240}$ resembles the sum of spectra of the two isolated fullerenes, thus illustrating the absence of strong plasmonic coupling between the fullerenes. The absence of interplay between the fullerenes was also confirmed by analyzing radial distribution of electron density of the system. The calculated spectrum of the $C_{20}@C_{60}$ buckyion differs significantly from the sum of the cross sections of the individual fullerenes because of strong geometrical dis-

tortion of the system and the related redistribution of valence electron density.

The contribution of collective electron excitations arising in individual fullerenes was evaluated by means of plasmon resonance approximation. It was demonstrated that the main features of the spectra, related to the formation of plasmon excitations, are well described by means of this model approach. An extension of the PRA formalism was presented, which allows for the study of collective electron excitations in multishell fullerenes under photon impact. In this extension, the behavior of electron densities on each molecule of the buckyonion is governed by the coupling parameter which is related to the geometry of the system. This parameter stands for the separation distance between the outer surface of the inner fullerene and the inner surface of the outer fullerene. As a case study, we have applied this formalism to $C_{60}@C_{240}$. The performed analysis revealed a shift of the plasmon resonance frequencies in the buckyonion compared to the case of the pristine fullerenes. On the other hand, this shift was not observed in the TDDFT-based calculations for C_{240} and $C_{60}@C_{240}$. Thus, a further analysis is required to understand the reason of this discrepancy and how the results obtained with the analytical model can be brought in line with those of the more elaborated method. This investigation is of significant interest because of little knowledge on the electronic properties of multishell fullerenes.

ACKNOWLEDGEMENTS

A.V. acknowledges the support by the FP7 Multi-ITN Project “ARGENT” (grant agreement no. 608163). A.V.K. acknowledges the support from the Alexander von Humboldt Foundation.

AUTHOR CONTRIBUTION STATEMENT

A.V. performed the calculations, analyzed the results and drafted the manuscript together with A.V.K. A.V.S. supervised the work. All authors discussed the results and commented on the manuscript.

Appendix A: Model description of the plasmon excitations in a multishell fullerene

The following general equation describes the dynamic variation, $\delta\rho(r)$, of the electron density in an arbitrary spherically symmetric system under the action of a

monochromatic uniform electric field \mathbf{E}_0 [4, 28]:

$$\begin{aligned} (\omega^2 - 4\pi\rho_0(r)) \delta\rho(r) + \frac{4\pi}{3} \rho'_0(r) \int_0^\infty r' g(r, r') \delta\rho(r') \\ = \rho'_0(r) \sqrt{\frac{4\pi}{3}} E_0. \end{aligned} \quad (A1)$$

Here $\rho_0(r)$ is the equilibrium distribution of electron density and ω is the field frequency. The function $g(r, r')$ is given by

$$g(r, r') = \Theta(r' - r) - 2 \left(\frac{r'}{r} \right)^3 \Theta(r - r') \quad (A2)$$

where $\Theta(x)$ is the Heaviside step function.

A multishell fullerene of an arbitrary level of complexity can be modeled as a set of n concentric spherical layers of finite width, i.e., a set of individual fullerenes. Let R_{1j} and R_{2j} ($R_{1j} < R_{2j}$) stand, respectively, for the inner and the outer radii of the j th fullerene ($j = 1, 2, \dots, n$) and $\Delta R_j = R_{2j} - R_{1j}$. The innermost fullerene is labeled with $j = 1$, and the outermost one with $j = n$.

Assuming the equilibrium distributions of electrons in each fullerene to be homogeneous, one writes the total equilibrium density $\rho_0(r)$ in the following form

$$\rho_0(r) = \sum_{j=1}^n \rho_{0j} \Theta(r - R_{1j}) \Theta(R_{2j} - r). \quad (A3)$$

Here, $\rho_{0j} = N_j/V_j$ with N_j standing for the number of valence electrons in the j th fullerene, and V_j for the volume of the spherical layer, $V_j = 4\pi/3 (R_{2j}^3 - R_{1j}^3)$. The quantity ρ_{0j} defines the plasmon frequency ω_{pj} :

$$\omega_{pj} = \sqrt{4\pi\rho_{0j}}. \quad (A4)$$

Since no volume plasmons can be excited under the action of a homogeneous dipole electric field [4, 45], the solution of equation (A1) can be sought in the following form:

$$\delta\rho(r) = \sum_{j=1}^n \left[\sigma_{1j} \delta(r - R_{1j}) + \sigma_{2j} \delta(r - R_{2j}) \right] \quad (A5)$$

where σ_{1j} and σ_{2j} are the variation of the charge densities on the inner and outer surfaces in the j th fullerene.

Using (A3) and (A5) in (A1) and carrying out the intermediate algebra, one derives

$$\begin{aligned} \sum_j \left[(\omega^2 \sigma_{1j} + \omega_{pj}^2 A_{1j}) \delta(r - R_{1j}) \right. \\ \left. + (\omega^2 \sigma_{2j} + \omega_{pj}^2 A_{2j}) \delta(r - R_{2j}) \right] \\ = \sqrt{\frac{4\pi}{3}} \frac{E}{4\pi} \sum_j \omega_{pj}^2 \left[\delta(r - R_{1j}) - \delta(r - R_{2j}) \right] \end{aligned} \quad (A6)$$

where

$$A_{1j} = -\frac{2}{3} \sum_{i < j} (\sigma_{1i} \alpha_{ij}^3 + \sigma_{2i} b_{ij}^3) - \frac{1}{3} (2\sigma_{1j} - \sigma_{2j}) + \frac{1}{3} \sum_{i > j} (\sigma_{1i} + \sigma_{2i}) \quad (\text{A7})$$

$$A_{2j} = \frac{2}{3} \sum_{i < j} (\sigma_{1i} a_{ij}^3 + \sigma_{2i} \beta_{ij}^3) + \frac{1}{3} (2\sigma_{1j} \xi_j^3 - \sigma_{2j}) - \frac{1}{3} \sum_{i > j} (\sigma_{1i} + \sigma_{2i}) \quad (\text{A8})$$

accompanied by

$$\alpha_{ij} = \frac{R_{1i}}{R_{1j}}, \quad \beta_{ij} = \frac{R_{2i}}{R_{2j}}, \quad a_{ij} = \frac{R_{1i}}{R_{2j}}, \quad b_{ij} = \frac{R_{2i}}{R_{1j}}, \quad \xi_j = \frac{R_{1j}}{R_{2j}}. \quad (\text{A9})$$

For each j , one equalizes the terms containing identical delta-functions on the left- and right-hand sides of (A6) and obtains the system of $2n$ equations. For a single fullerene ($n = 1$), this system reduces to the equations presented and analyzed in Ref. [4].

1. System of two concentric fullerenes, $C_{N_1}@C_{N_2}$

For $n = 2$, the system of equations (A6) can be explicitly written in the matrix form:

$$\mathbf{D} \begin{pmatrix} \sigma_{11} \\ \sigma_{21} \\ \sigma_{12} \\ \sigma_{22} \end{pmatrix} = \begin{pmatrix} -\omega_{p1}^2 f \\ \omega_{p1}^2 f \\ -\omega_{p2}^2 f \\ \omega_{p2}^2 f \end{pmatrix} \quad (\text{A10})$$

where $f = -\sqrt{4\pi/3}E_0/4\pi$, and \mathbf{D} denotes the matrix

$$\mathbf{D} = \begin{pmatrix} D_{11} & D_{12} \\ D_{21} & D_{22} \end{pmatrix}. \quad (\text{A11})$$

The diagonal blocks

$$D_{jj} = \begin{pmatrix} \omega^2 - 2\lambda_j & \lambda_j \\ 2\lambda_j \xi_j^3 & \omega^2 - \lambda_j \end{pmatrix}, \quad j = 1, 2 \quad (\text{A12})$$

describe the excitations in isolated fullerenes, whereas the blocks D_{12} and D_{21} are due to the interaction between the fullerenes:

$$D_{12} = \begin{pmatrix} \lambda_1 & \lambda_1 \\ -\lambda_1 & -\lambda_1 \end{pmatrix}, \quad D_{21} = \begin{pmatrix} -2\lambda_2 \alpha_{12}^3 & -2\lambda_2 b_{12}^3 \\ 2\lambda_2 a_{12}^3 & 2\lambda_2 \beta_{12}^3 \end{pmatrix}. \quad (\text{A13})$$

In these formulae $\lambda_j = \omega_{pj}^2/3$.

The determinant $|\mathbf{D}|$ is equal to

$$|\mathbf{D}| = |\mathbf{D}_{11}| |\mathbf{D}_{22}| - 2\lambda_1 \lambda_2 (1 - \xi_1^3) (1 - \xi_2^3) (\omega^2 - 2\lambda_1)(\omega^2 - \lambda_2) b_{12}^3, \quad (\text{A14})$$

where $b_{12} = R_{21}/R_{12}$ and $|\mathbf{D}_{jj}|$ are determinants of the matrices \mathbf{D}_{jj} :

$$|\mathbf{D}_{jj}| = (\omega^2 - \omega_1^{(j)2}) (\omega^2 - \omega_2^{(j)2}) \quad (\text{A15})$$

where

$$\omega_1^{(j)} = \omega_{pj} \sqrt{\frac{3-p_j}{6}}, \quad \omega_2^{(j)} = \omega_{pj} \sqrt{\frac{3+p_j}{6}} \quad (\text{A16})$$

with $p_j = \sqrt{1 + 8\xi_j^3}$. The frequencies (A16) correspond to the symmetric, $\omega_1^{(j)} \equiv \omega_s^{(j)}$, and antisymmetric, $\omega_2^{(j)} \equiv \omega_a^{(j)}$, modes of the surface plasmon oscillations in a pristine C_{N_j} fullerene. For $C_{N_1}@C_{N_2}$, the resonance frequencies ω_k ($k = 1, 2, 3, 4$) are found as the roots of the secular equation

$$|\mathbf{D}_{11}| |\mathbf{D}_{22}| - 2\lambda_1 \lambda_2 (1 - \xi_1^3) (1 - \xi_2^3) (\omega^2 - 2\lambda_1)(\omega^2 - \lambda_2) b_{12}^3 = 0. \quad (\text{A17})$$

In the limit of uncoupled fullerenes, the secular equation reduces to $|\mathbf{D}_{11}| |\mathbf{D}_{22}| = 0$ resulting in (A16). Formally, this limit corresponds to $b_{12} = 0$ in equation (A17). Indeed, this parameter is the only one which couples the characteristics of both fullerenes.

Appendix B: Application to $C_{60}@C_{240}$

A $C_{60}@C_{240}$ buckyonion can be modeled as a set of two concentric spherical shells of the same width ΔR , see Fig. 2. The inner and outer radii of the fullerenes as well as the related parameters are summarized in Table I. In what follows, the indices $j = 1, 2$ labels the C_{60} and C_{240} fullerenes, respectively.

Figure 2 and the data presented in Table I suggest that the values of electron densities, ρ_{0j} , in both fullerenes are essentially the same, yielding the discrepancy of ca. 1.5%. Assuming $\rho_{01} = \rho_{02}$ one equalizes the plasmon frequencies:

$$\omega_{p1}^2 = \omega_{p2}^2 \equiv \omega_p^2 \quad (\text{B1})$$

with $\omega_p \approx 37.2$ eV.

This relation allows one to solve the secular equation analytically. Indeed, Eq. (A17), being written in terms of the variable $\eta = \omega^2/\omega_p^2 - 1/2$, can be further reduced to the bi-quadratic one resulting in the following set of

ω_k :

$$\begin{cases} \frac{\omega_1^2}{\omega_p^2} = \frac{2}{9}s_1s_2 \left[\frac{s_1+s_2}{s_1s_2} - b^3 - \sqrt{(b^3+\chi_-)(b^3+\chi_+)} \right] \\ \frac{\omega_2^2}{\omega_p^2} = \frac{2}{9}s_1s_2 \left[\frac{s_1+s_2}{s_1s_2} - b^3 + \sqrt{(b^3+\chi_-)(b^3+\chi_+)} \right] \\ \omega_3^2 = \omega_p^2 - \omega_2^2 \\ \omega_4^2 = \omega_p^2 - \omega_1^2 \end{cases} \quad (B2)$$

where $b = R_2(C_{60})/R_1(C_{240}) \approx 0.67$, $s_j = 1 - \xi_j^3$ and $\chi_{\pm} = (\xi_1^{3/2} \pm \xi_2^{3/2})^2 / s_1s_2$. For the purpose of self-consistency, thus calculated values of ω_k^2 ($k = 1 \dots 4$) should be augmented by the additional term ω_0^2 , introduced and explained in Section II B.

TABLE II. Resonance frequencies calculated for $b = 0$ (the limit of uncoupled fullerenes) and for $b = 0.67$ which corresponds to the model geometry of $C_{60}@C_{240}$.

b	ω_1 (eV)	ω_2 (eV)	ω_3 (eV)	ω_4 (eV)
0	16.6	19.8	34.6	35.7
0.67	14.5	20.7	34.1	36.5

Carrying out the limit $b = 0$ in Eq. (B2), one relates ω_k to the frequencies of the symmetric and antisymmetric surface plasmon modes in pristine C_{60} and C_{240} :

$$\begin{aligned} \omega_1|_{b=0} &= \omega_s(C_{240}), & \omega_2|_{b=0} &= \omega_s(C_{60}), \\ \omega_3|_{b=0} &= \omega_a(C_{60}), & \omega_4|_{b=0} &= \omega_a(C_{240}). \end{aligned} \quad (B3)$$

The formal dependence of ω_k on b is presented in Fig. 8 where the vertical line marks the value $b \approx 0.67$ consistent with the data from Table I. The values of ω_k for this b are listed in Table II where they are compared with the resonance frequencies in pristine C_{60} and C_{240} , defined by Eq. (9).

Writing the determinant of D (see Eq. (A11)) as $|D| = \prod_{k=1}^4 (\omega^2 - \omega_k^2)$, one resolves Eq. (A10) with respect to the surface charge densities. The result reads:

$$\sigma_{11} = \frac{x^3 - x^2}{3|D|} \omega_p^8 E_0 \quad (B4)$$

$$\sigma_{21} = -\frac{x^3 - \lambda(3 + 2s_1)x^2 + 6\lambda^2 s_1 x}{3|D|} \omega_p^8 E_0 \quad (B5)$$

$$\sigma_{12} = \frac{x^3 - \lambda(3 + 2b^3 s_1)x^2 + 2\lambda^2(1 + 2b^3)s_1 x}{3|D|} \omega_p^8 E_0 \quad (B6)$$

$$\begin{aligned} \sigma_{22} = & -\frac{1}{3|D|} \left[x^3 + \lambda(2(a^3 - \beta^3 - s_2) - 3)x^2 \right. \\ & + 2\lambda^2(3(\beta^3 - a^3 + s_2) + \alpha^3 - b^3 + s_1)x \\ & \left. - 4\lambda^3(\alpha^3 + \beta^3 - a^3 - b^3 + s_1s_2) \right] \omega_p^8 E_0. \end{aligned} \quad (B7)$$

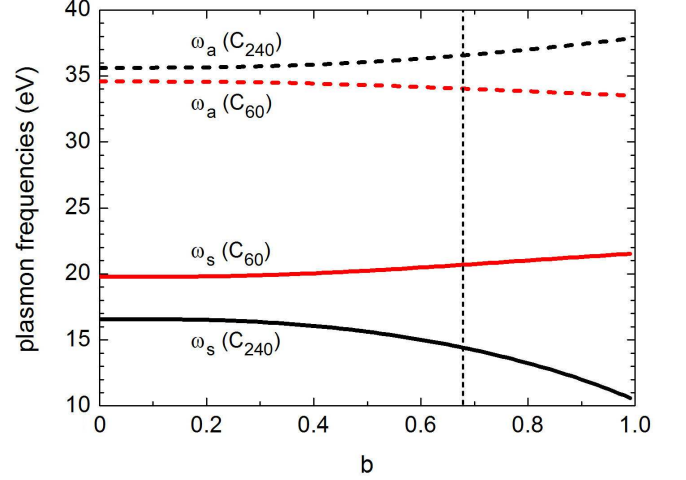


FIG. 8. Resonance frequencies $\omega_{1,\dots,4}$ as formal functions of the coupling parameter b . The frequencies were calculated using Eq. (B2) and augmented by the term ω_0^2 as described in the main text. The curves correspond to the plasmon frequency $\omega_p = 37.2$ eV. Dashed vertical line marks the value $b = 0.67$ which is consistent with the chosen inner and outer radii of the fullerenes, see Table I. In the limit $b = 0$, the frequencies $\omega_{1,\dots,4}$ correspond to the indicated frequencies of the symmetric and antisymmetric surface plasmon modes in C_{60} and C_{240} .

In these formulae, $x = \omega^2/\omega_p^2$, $\lambda = 1/3$, $s_j = 1 - \xi_j^3$, and

$$\begin{aligned} \alpha &= \frac{R_{11}}{R_{12}} = 0.43, & \beta &= \frac{R_{21}}{R_{22}} = 0.54, \\ a &= \frac{R_{11}}{R_{22}} = 0.35, & b &= \frac{R_{21}}{R_{12}} = 0.67, \end{aligned} \quad (B8)$$

with R_{1j} and R_{2j} standing for the inner and outer radii of C_{60} ($j = 1$) and C_{240} ($j = 2$).

Once the surface densities are found, one calculates the induced dipole moment d :

$$\begin{aligned} d = \int r^3 & \left[\sigma_{11}\delta(r - R_{11}) + \sigma_{21}\delta(r - R_{21}) \right. \\ & \left. + \sigma_{12}\delta(r - R_{12}) + \sigma_{22}\delta(r - R_{22}) \right] \mathbf{r}. \end{aligned} \quad (B9)$$

Dividing d by E_0 , one determines the dipole polarizability $\alpha(\omega)$ of the system. The final result for $\alpha(\omega)$ can be written as a sum of four resonance terms:

$$\alpha(\omega) = \sum_{k=1}^4 \frac{\mathcal{N}_k}{\omega_k^2 - \omega^2}. \quad (B10)$$

The oscillator strengths, \mathcal{N}_k , associated with the resonances $\omega = \omega_k$, are

$$\mathcal{N}_k = \frac{R_{22}^3}{3} \omega_p^2 A_k, \quad (B11)$$

where

$$\begin{aligned} A_1 &= [(\kappa_{23} - \kappa_{14})(X_1 - X_4)]^{-1} \mathcal{A}(X_1), \\ A_2 &= [(\kappa_{23} - \kappa_{14})(X_3 - X_2)]^{-1} \mathcal{A}(X_2), \\ A_3 &= [(\kappa_{23} - \kappa_{14})(X_2 - X_3)]^{-1} \mathcal{A}(X_3), \\ A_4 &= [(\kappa_{23} - \kappa_{14})(X_4 - X_1)]^{-1} \mathcal{A}(X_4). \end{aligned} \quad (\text{B12})$$

Here $X_k = \omega_k^2 / \omega_p^2$, $\kappa_{14} = X_1 X_4$, $\kappa_{23} = X_2 X_3$, and

$$\mathcal{A}(X_k) = a_3 X_k^3 + a_2 X_k^2 + a_1 X_k + a_0, \quad (\text{B13})$$

with

$$\begin{aligned} a_3 &= s_2 + b^3 s_1 - b^3 s_1 s_2, \quad a_2 = -\frac{5a_3}{3}, \\ a_1 &= \frac{2a_3}{3} - \frac{3a_0}{2}, \quad a_0 = -\frac{4}{27}(1 - b^3)s_1 s_2. \end{aligned} \quad (\text{B14})$$

Thus defined oscillator strengths satisfy the sum rule $\sum_{j=1}^4 \mathcal{N}_j = N_1 + N_2 = 1200$, that is the total number of delocalized electrons in $\text{C}_{60}@\text{C}_{240}$.

In the limit of uncoupled fullerenes, the oscillator strengths \mathcal{N}_2 and \mathcal{N}_3 reduce, respectively, to $N_1(p_1 +$

$1)/2p_1$ and $N_1(p_1 - 1)/2p_1$ (where $p_1 = \sqrt{1 + 8\xi_1^3}$) which stand for the number of electrons in pristine C_{60} participating in the symmetric and antisymmetric oscillation modes [4, 56]. The quantities \mathcal{N}_1 and \mathcal{N}_4 reduce to those in pristine C_{240} .

More accurate treatment of $\alpha(\omega)$ must account for damping of the plasmon oscillations. Formally, this can be achieved by introducing the finite widths, Γ_k , in the denominators in (B10): $\omega_k^2 - \omega^2 \rightarrow \omega_k^2 - \omega^2 - i\omega\Gamma_k$. The widths can be calculated considering the decay of the collective excitation mode into the incoherent sum of single-electron excitations [57]. With the widths introduced, the photoionization cross section of a buckyonion is found from

$$\sigma(\omega) = \frac{4\pi\omega}{c} \text{Im} \alpha(\omega) \quad (\text{B15})$$

where c is the speed of light and the polarizability α is defined by Eq. (B10).

-
- [1] P. Wopperer, P.M. Dinh, P.-G. Reinhard, E. Suraud, Phys. Rep. **562**, 1 (2015)
 - [2] F. Lépine, J. Phys. B: At. Mol. Opt. Phys. **48**, 122002 (2015)
 - [3] A.V. Solov'yov, Int. J. Mod. Phys. B **19**, 4143 (2005)
 - [4] A.V. Verkhovtsev, A.V. Korol, A.V. Solov'yov, Eur. Phys. J. D **66**, 253 (2012)
 - [5] A.L.D. Kilcoyne et al., Phys. Rev. Lett. **105**, 213001 (2010)
 - [6] S. Biswas, L.C. Tribedi, Phys. Rev. A **92**, 060701(R) (2015)
 - [7] I.V. Hertel, H. Steger, J. de Vries, B. Weissner, C. Menzel, B. Kamke, and W. Kamke, Phys. Rev. Lett. **68**, 784 (1992)
 - [8] J. Berkowitz, J. Chem. Phys. **111**, 1446 (1999)
 - [9] S.W.J. Scully *et al.*, Phys. Rev. Lett. **94**, 065503 (2005)
 - [10] L.G. Gerchikov, P.V. Efimov, V.M. Mikoushkin, A.V. Solov'yov, Phys. Rev. Lett. **81**, 2707 (1998)
 - [11] P. Bolognesi, A. Ruocco, L. Avaldi, A.V. Verkhovtsev, A.V. Korol, A.V. Solov'yov, Eur. Phys. J. D **66**, 254 (2012)
 - [12] M. Schüler, J. Berakdar, Y. Pavlyukh, Phys. Rev. A **92**, 021403(R) (2015)
 - [13] A. Verkhovtsev, S. McKinnon, P. de Vera, E. Surdutovich, S. Guatelli, A.V. Korol, A. Rosenfeld, A.V. Solov'yov, Eur. Phys. J. D **69**, 116 (2015)
 - [14] K. K. Baral *et al.*, Phys. Rev. A **93**, 033401 (2016)
 - [15] E. Brun, P. Cloutier, C. Sicard-Roselli, M. Fromm, L. Sanche, J. Phys. Chem. B **113**, 10008 (2009)
 - [16] A.V. Verkhovtsev, A.V. Korol, A.V. Solov'yov, Phys. Rev. Lett. **114**, 063401 (2015)
 - [17] D. Ugarte, Nature **359**, 707 (1992)
 - [18] D. Ugarte, Carbon **33**, 989 (1995)
 - [19] S. Iglesias-Groth, A. Ruiz, J. Bretón, J.M. Gomez Llorente, J. Chem. Phys. **118**, 7103 (2003)
 - [20] R.R. Zope, J. Phys. B: At. Mol. Opt. Phys. **41**, 085101 (2008)
 - [21] V.K. Dolmatov, P. Brewer, S.T. Manson, Phys. Rev. A **78**, 013415 (2008)
 - [22] M.Ya. Amusia, L.V. Chernysheva, E.Z. Liverts, Phys. Rev. A **80**, 032503 (2009)
 - [23] A. Ruiz, J. Bretón, J.M. Gomez Llorente, J. Chem. Phys. **120**, 6163 (2003)
 - [24] M.A. McCune, R. De, M.E. Madjet, H.S. Chakraborty, S.T. Manson, J. Phys. B: At. Mol. Opt. Phys. **44**, 241002 (2011)
 - [25] G. Casella, A. Bagno, G. Saielli, Phys. Chem. Chem. Phys. **15**, 18030 (2013)
 - [26] T. Cabioch, J.C. Girard, M. Jaouen, M.F. Denanot, G. Hug, Europhys. Lett. **38**, 471 (1997)
 - [27] M. Chhowalla, H. Wang, N. Sano, K.B.K. Teo, S.B. Lee, G.A.J. Amaratunga, Phys. Rev. Lett. **90**, 155504 (2003)
 - [28] J.-P. Connerade, A.V. Solov'yov, Phys. Rev. A **66**, 013207 (2002)
 - [29] B. Walker, A.M. Saitta, R. Gebauer, S. Baroni, Phys. Rev. Lett. **96**, 113001 (2006)
 - [30] D. Rocca, R. Gebauer, Y. Saad, S. Baroni, J. Chem. Phys. **128**, 154105 (2008)
 - [31] O.B. Malcioğlu, R. Gebauer, D. Rocca, S. Baroni, Comp. Phys. Commun. **182**, 1744 (2011)
 - [32] B. Walker, R. Gebauer, J. Chem. Phys. **127**, 164106 (2007)
 - [33] M.J. Frisch *et al.*, Gaussian 09 Revision A.02, Gaussian Inc. Wallingford CT, 2009
 - [34] J.P. Perdew, A. Zunger, Phys. Rev. B **23**, 5048 (1981)
 - [35] P. Giannozzi *et al.*, J. Phys.: Cond. Mat. **21**, 395502 (2009)
 - [36] A.M. Rappe, K.M. Rabe, E. Kaxiras, J.D. Joannopoulos, Phys. Rev. B **41**, 1227 (1990); Phys. Rev. B **44**, 13175 (1991) (erratum)

- [37] Ph. Lambin, A.A. Lucas, J.-P. Vigneron, Phys. Rev. B **46**, 1794 (1992)
- [38] D. Östling, P. Apell, A. Rosen, Europhys. Lett. **21**, 539 (1993)
- [39] S. Lo, A.V. Korol, A.V. Solov'yov, J. Phys. B: At. Mol. Opt. Phys. **40**, 3973 (2007)
- [40] A.V. Verkhovtsev, A.V. Korol, A.V. Solov'yov, P. Bolognesi, A. Ruocco, L. Avaldi, J. Phys. B: At. Mol. Opt. Phys. **45**, 141002 (2012)
- [41] A.V. Verkhovtsev, A.V. Korol, A.V. Solov'yov, J. Phys.: Conf. Ser. **438**, 012011 (2013)
- [42] A.V. Verkhovtsev, A.V. Korol, A.V. Solov'yov, Phys. Rev. A **88**, 043201 (2013)
- [43] P. Apell, D. Östling, G. Mukhopadhyay, Solid State Commun. **87**, 219 (1993)
- [44] B. Vasvári, Z. Phys. B **100**, 223 (1996)
- [45] A.V. Korol, A.V. Solov'yov, Phys. Rev. Lett. **98**, 179601 (2007)
- [46] A.V. Verkhovtsev, R.G. Polozkov, V.K. Ivanov, A.V. Korol, A.V. Solov'yov, J. Phys. B: At. Mol. Opt. Phys. **45**, 215101 (2012)
- [47] T. Lu, F. Chen, J. Comput. Chem. **33**, 580 (2012)
- [48] R.R. Zope, S. Bhusal, L. Basurto, T. Baruah, K. Jackson, J. Chem. Phys. **143**, 084306 (2015)
- [49] B.P. Kafle, H. Katayanagi, M. Prodhan, H. Yagi, C. Huang, K. Mitsuke, J. Phys. Soc. Jpn. **77**, 014302 (2008)
- [50] S. Saito, A. Oshiyama, Phys. Rev. Lett. **66**, 2637 (1991)
- [51] A.V. Korol, A.V. Solov'yov, *Polarization Bremsstrahlung*, Springer Series on Atomic, Optical, and Plasma Physics, Vol. 80 (Springer, 2014)
- [52] L. Türker, J. Molec. Struct. (Theochem) **545**, 207 (2001)
- [53] F. Liu, L. Meng, S. Zheng, J. Molec. Struct. (Theochem) **725**, 17 (2005)
- [54] P. Schwerdtfeger, L.N. Wirz, J. Avery, WIREs Comput. Mol. Sci. **5**, 96 (2015)
- [55] M.A. Fox and J.K. Whitesell, *Organic Chemistry* 3rd ed. (Jones & Bartlett Publishers, Sudbury, MA, 2004)
- [56] S. Lo, A.V. Korol, A.V. Solov'yov, Phys. Rev. A **79**, 063201 (2009)
- [57] L.G. Gerchikov, A.N. Ipatov, R.G. Polozkov, A.V. Solov'yov, Phys. Rev. A **62**, 043201 (2000)